Numerical Investigations of Variable Pitch Straight-Bladed H-Darrieus VAWT

Temesgen Abriham Miliket[1(✉)], Mesfin Belayneh Ageze[2], and Muluken Temesgen Tigabu[1]

[1] Faculty of Mechanical and Industrial Engineering, Bahir Dar Energy Centre, Bahir Dar Institute of Technology, Bahir Dar University, Bahir Dar, Ethiopia
[2] Addis Ababa Energy Center, Addis Ababa University, Addis Ababa, Ethiopia

Abstract. In this paper, we aim to develop low cost effective model for evaluating the aerodynamic design and performance of small scale straight blade H-Darrieus vertical axis wind turbine (VAWT). To optimize the rotor design the blades are modeled with variable pitch angle (β) configurations. To this end, DMST model was used to determine optimum pitch configuration at the minimum possible tip speed ratio (λ). Once the optimal design point was obtained, 2D unsteady computational fluid dynamics (CFD) simulation was carried out in order to describe the flow physics of the rotor. The power coefficient (Cp) obtained in DMST model was 0.464 which is in agreement with the present CFD simulation result computed by SST k-ω model (i.e. Cp = 0.4537) and wind tunnel experimental findings from literatures. This implies the performance of straight blade H-Darrieus VAWT with VP design is 37.2% better than one with the fixed pitch (β = 0°) blades. Hence, the present study delineates the performance of H-Darrieus wind turbine is dependent upon the turbine parameters, airfoil profile and desired blade pitch angle for sustainable power generation.

Keywords: Vertical axis wind turbine · Variable pitch blade · Double-multiple stream tube model · Computational fluid dynamics · Self starting · Power coefficient

1 Introduction

The wind is one of the most potential renewable energy resources in the world which utilizes wind turbines as a conversion machine. Among the types of wind turbines, H-Darrieus VAWT is the most popular one which yields higher power output at high wind speed. Despite this, the performance of the H-Darrieus wind turbine is relatively very low at low wind speed [1, 2]. Hence, attempts are devoted to exploring to enhance the aerodynamic performance of the rotor [3]. Associated with the rotor blade design, airfoil selection is the primary considerations. Symmetrical NACA-series are frequently used

M. L. Berihun (Ed.): ICAST 2021, LNICST 412, pp. 565–583, 2022.
https://doi.org/10.1007/978-3-030-93712-6_38

for straight blade H-Darrieus VAWT design [3]. However, these airfoil blades generate negative Cp at a low Reynolds number [4]. Contrarily, the power production of high solidity turbines became independent at high arbitrary Reynolds numbers [5]. To improve VAWT performance-enhanced shape airfoils such as S1046 airfoil become more effective for blade designs [6]. Hence, to afford enhanced wind turbine at low Reynolds number, blades to arm configuration also a crucial consideration. Based on the movement of the blade concerning the supporting strut, the blade of a wind turbine can be classified as either fixed or variable pitch. In a fixed pitch (FP) H-Darrieus wind turbine; airfoil blades, supporting struts, and tower are the main components [7]. The system doesn't need any blade pitch control mechanism rather it helps to minimize investment costs. However, it experienced much stalled time at a low tip speed ratio (TSR) [8], which may lead to catastrophic failure. Hence, researchers are coming with a variable pitch (VP) blade design that maintains the blade's angle of attacks (AoA) at required positions and reducing stalls. These designs are superior to overcome the self-starting problems and provide higher torque coefficients by allowing the blades to pitch cyclically [9, 10]. To allow the blade at optimum AoA through the rotor azimuth angle, the system can be managed by using either passive or active control systems [11, 12]. However small-scale VAWT are more fundamental with active pitch controls.

A wide range of analytical and computational studies has been carried out about the performance predictions of VAWT. However, due to the aerodynamic complexity of the H-Darrieus rotor research efforts are perusing enhanced modeling methods up-to-date. To acquire such analysis superimposing various model become a typical choice for robust performance investigations. DMST model developed by I.Paraschivoiu [13], is the combination of multiple stream tube (MST) model and double actuator disk (AD) theory [14, 15]. These models divide the rotor into upwind and downwind halves and account for any induction factor when VAWT is subjected to aerodynamic loadings [14]. DMST model used in [16], VP-VAWT with smaller AoA widen the rotor performance azimuth zone. DMST model and Prandtl's mathematics were used to evaluate the blade tip loss of FP and VP VAWT at rated TSR [17]. The result shows VP-approach achieves 18.9% performance growth. Also, detailed understandings of CFD helps to predict an accurate flow physics of VAWT. However, the selection of the physical model and turbulence affect the accuracy of the results [18]. Except for eddy simulations, all turbulence models in CFD have similar transport equations for turbulent kinetic energy (k) and turbulent dissipation rate(ε) [19]. But in the eddy simulation, the Prandtl numbers govern the turbulent diffusion and dispassion rate. The k-ε turbulence model is the most common turbulence model used in industrial applications. The main problems observed in k-ε turbulence models are not efficient to compute near-wall boundary flow with adverse pressure gradients [18]. However, the k-ω model has a low computational cost and better computational accuracy than the k-ε model. Besides that, the main drawback of the k-ω turbulence model is hard to converge and sensitive to initial conditions.

Hence, a robust turbulence model is required to capture near-wall and far-wall flow conditions for the accurate performance predictions of the turbine. The freestream inflow which is far away from the wall boundary is used the formulated SST k-ω turbulence model which can accurately be calculated for the separation [20]. Hence, SST k-ω turbulence model can achieve good results because of its capability of capturing proper behaviour in the near-wall layers or shear stress transports of the fluid and separated flow regions [21]. In the present study, the performances enhancement of straight-bladed H-Darrieus VAWT is carried out through DMST and CFD models.

2 Aerodynamic Analysis of H-Darrieus Rotor

The wind velocity at the rotor plane of each tandem disk can be defined by the induction factor [22, 23]. And also the wake velocity of upwind, equilibrium, and downwind half of the rotor can be determined reduced by induction factors [24, 25]. Hence the axial velocity through the upwind and downwind sides of the disks can be written as $V_e < V_i < V_\infty$ and $V_w < V_i^{'} < V_e$ respectively. The main mathematical models which need for the DMST analysis are presented in this section, the details are available in [26] (Fig. 1).

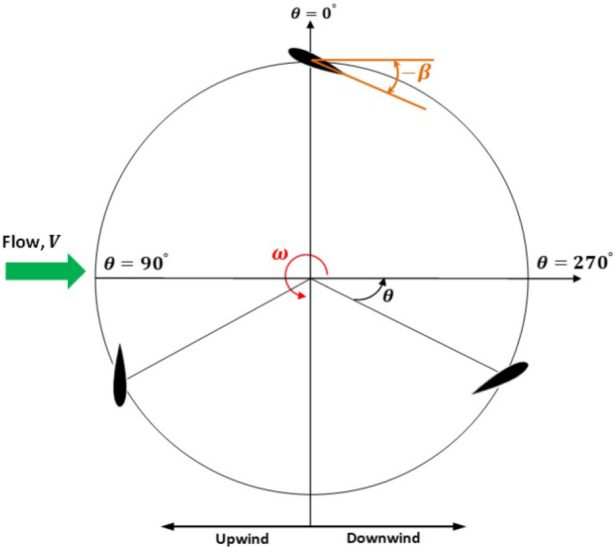

Fig. 1. Schematic of variable pitch VAWT [27].

Upwind induced velocity:

$$V = aV_{\infty} \tag{1}$$

Equilibrium induced velocity;

$$V_e = (2a - 1)V_{\infty} \tag{2}$$

Downwind induced velocity;

$$W_w = a'(2a - 1)V_{\infty} \tag{3}$$

Tip Speed Ratio (λ);

$$\lambda = \frac{\omega_r R}{V_{\infty}} \tag{4}$$

The angle of attack (α);

$$\alpha = \tan^{-1}\left(\frac{(1-a)\sin(\theta)}{\lambda + (1-a)\cos(\theta)}\right) \tag{6}$$

When we consider the blade pitch angle, the modified angle of attack [16, 17] can be written as:

The modified angle of attack (α_{mdf});

$$\alpha_{mdf} = \alpha - \beta(\theta) \tag{7}$$

Blade pitch angle (β);

$$\beta(\theta) = \beta_o \sin(\theta) \tag{8}$$

Normal force coefficient (CN);

$$CN = CL\cos(\alpha) + CD\sin(\alpha) \tag{9}$$

Tangential force coefficient (CT);

$$CT = CL\sin(\alpha) - CD\cos(\alpha) \tag{10}$$

Average thrust coefficient (C_T);

$$C_T = \left(\frac{Nc}{R}\right)\left(\frac{1}{2\pi}\right)\left(\frac{W}{V_{\infty}}\right)^2\left[CN - CT\left(\frac{\cos(\theta)}{\sin(\theta)}\right)\right] \tag{11}$$

Interference factor (f);

$$f = \frac{Nc}{8\pi R} \int_{-\pi/2}^{\pi/2} \left(\frac{W}{V_\infty}\right)^2 (CN\sin(\theta) - CT\cos(\theta))d\theta \tag{12}$$

Axial induction factor (a);

$$a = \frac{\pi}{\pi + f} \tag{13}$$

Instantaneous torque (Qinst);

$$Q_{inst} = \frac{1}{2} C_T \rho c R W^2 h \tag{14}$$

Average instantaneous torque (Qavg);

$$Q_{avg} = \frac{N}{2\pi} \int_{-\pi/2}^{\pi/2} Q_{inst} d\theta \tag{15}$$

Power coefficient (CP);

$$C_P = \lambda C_m \tag{16}$$

Where Cm is the turbine moment coefficients (Fig. 2).

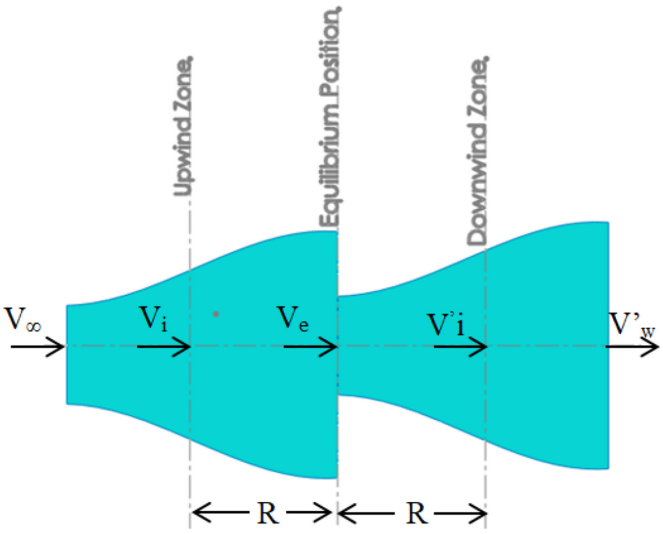

Fig. 2. Illustration of DMST model.

2.1 Double Multiple Stream Tube (DMST) Analysis

2.2 Computational Analysis

Governing Equations. A 2D pressure-based U-RANS formulation is used for numerical simulation and is a suitable solver for time-dependent analysis [28]. Semi-Implicit Method for Pressure Linked Equations (SIMPLE) algorithms with Second-order upwind scheme is selected for the spatial discretization method using finite volume analysis [29], for momentum, energy, and turbulence, as well as the bounded second-order implicit, are executed for the transient formulation [30]. Assuming the flow in the wind turbine is incompressible, continuity and momentum equation [31, 32] of unsteady flow can be written in the formula as in equations (16) and (17):

$$\nabla.\left(\rho\overrightarrow{V}\right) = 0 \tag{17}$$

$$\frac{\partial(\rho u)}{\partial t} + \nabla.\left(\rho u\overrightarrow{V}\right) = \frac{\partial p}{\partial x} + \frac{\partial \tau_{xx}}{\partial x} + \frac{\partial \tau_{yx}}{\partial y} \tag{18}$$

$$\frac{\partial(\rho v)}{\partial t} + \nabla.\left(\rho v\overrightarrow{V}\right) = -\frac{\partial p}{\partial y} + \frac{\partial \tau_{yy}}{\partial y} + \frac{\partial \tau_{xy}}{\partial x} \tag{19}$$

Turbulence Modeling. In the present work SST-kω model introduced by [33] was used due to its better accuracy [34]. The general mathematical formulations of the SST-kω model [31], can be written as Eq. (20)

$$\frac{\partial(\rho k)}{\partial t} + \frac{\partial(\rho k u_i)}{\partial x_i} = \frac{\partial}{\partial x_j}\left(\Gamma_k \frac{\partial k}{\partial x_j}\right) + G_k - Y_k + S_K \tag{20}$$

$$\frac{\partial(\rho\omega)}{\partial t} + \frac{\partial\left(\rho\omega u_j\right)}{\partial x_i} = \frac{\partial}{\partial x_j}\left(\Gamma_\omega \frac{\partial \omega}{\partial x_j}\right) + G_\omega - Y_\omega + S_\omega \tag{21}$$

$$\Gamma_\omega = \mu + \frac{\mu_t}{\sigma_\omega} \tag{22}$$

$$\Gamma_k = \mu + \frac{\mu_t}{\sigma_k} \tag{23}$$

Where μ_t is the turbulent viscosity, σ_k and σ_ω are the turbulent Prandtl numbers for k and ω respectively.

$$\mu_t = \frac{\rho k}{\omega} \frac{1}{\max\left[\frac{1}{a^*}, \frac{SF_2}{a_1 \omega}\right]} \tag{24}$$

Where S (k,ω) is the strain rate magnitudes.

3 Methodology

3.1 DMST Model Solver Procedure

To calculate various parameters of the turbine the above simplified referred Eqs. (1) up to (16) are formulated with computer code developed in MATLAB R2019a software. Figure 3 illustrates the working loops of DMST algorisms; each half of the stream tube which classify into three main consecutive parameters i.e. impute parameters, calculated parameters, and output parameters. To begin the calculation process, first importing S1046 airfoil coordinate taken from University of Illinois at Urbana-champaign (UIUC) airfoil database to the foil tool and then the airfoils are imported to Q-blade to export the lifts (CL) and drag (CD) coefficients at different local Reynolds number with a corresponding angle of attack. To find intermediate working values, a linear interpolation method was used [35]. Following the input parameters, the calculations are initialized and an iterative process was used in the range $-\frac{\pi}{2} \leq \theta_{up} \leq \frac{\pi}{2}$ the upstream and downstream $\frac{\pi}{2} \leq \theta_{dw} \leq \frac{3\pi}{2}$ half interference factors of the turbine are computed until convergence is reached. Finally, optimum turbine performances are obtained based on the output parameters followed by the whole process.

3.2 Computational Fluid Dynamics (CFD) Method

ANSYS 19.2® fluent® commercial solver was used to understand the level of accuracy of the RANS equations using the SST-k-ω model in predicting the aerodynamic performance of the present model. To achieve computational accuracy 2D unsteady simulation was used for relevant H-Darrieus rotors computation [25]. Figure 4 demonstrates the geometry layout for the present simulation based on the information in Table 1.

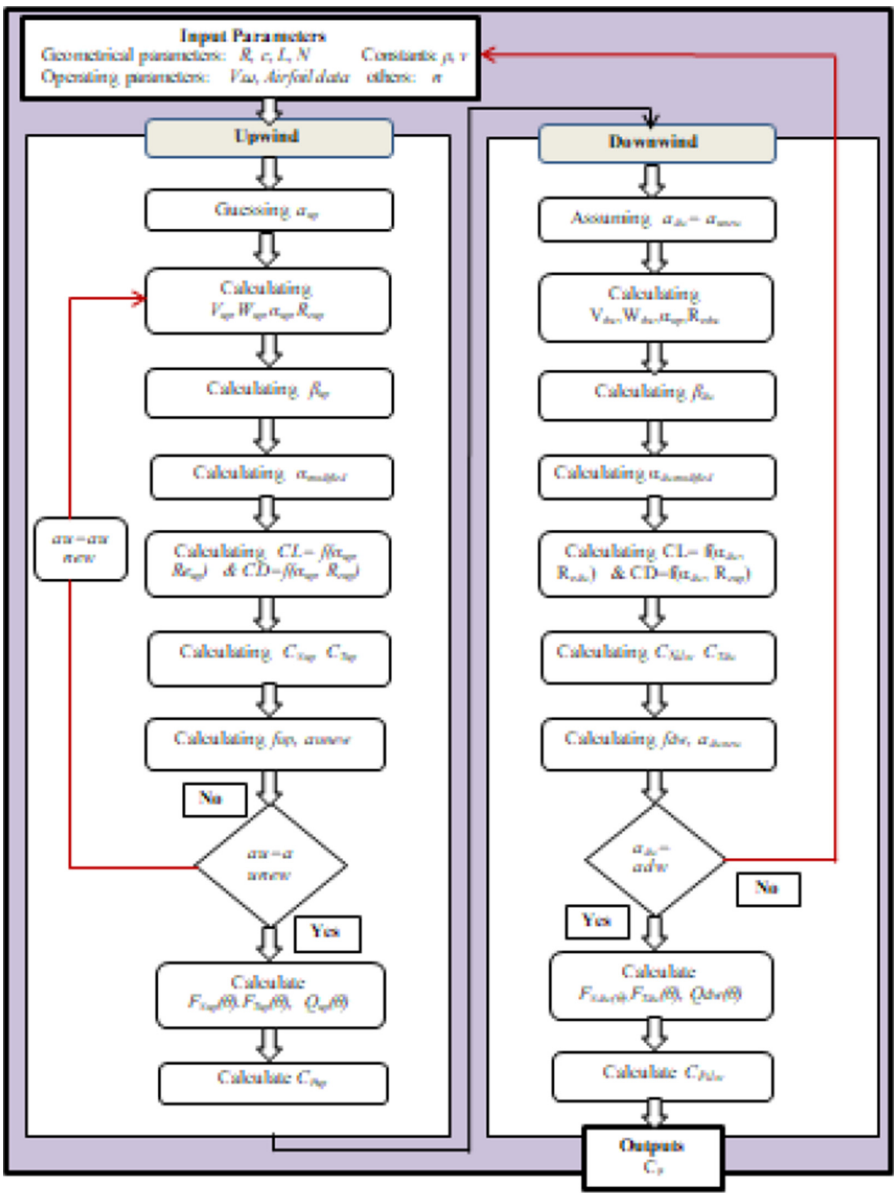

Fig. 3. DMST model algorism.

Table 1. Simulation parameters.

Parameters	Dimensions
Airfoil	S1046
c	0.09
R	1
N	3
Inlet velocity	9
Simulation type	2D unsteady
Model	SST-$k\omega$
Pitching mechanism	Fixed and variable

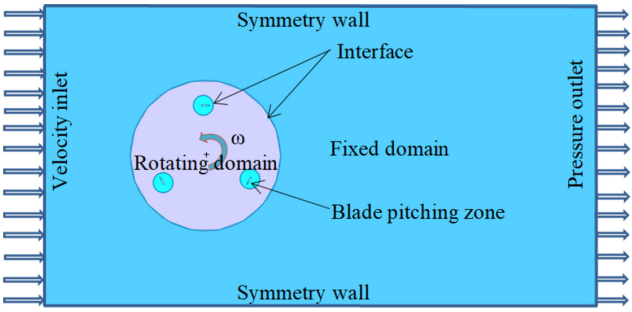

Fig. 4. Model geometry

Mesh Independence Study. To get improved quality of mesh spatial discretization, the triangular mesh has been taken place in the three sub-domains i.e fixed domain, rotating domain, and blades edge seen in Fig. 5. To obtain the grid-independent result, positioning the shape of surface mesh refinement on the computational sub-domain was done [30]. This can be achieved the relative velocity of the blade reaches a maximum value when the first mesh cell distance becomes at the nearest position. Hence the meshes are metric by the maximum Skewness value was 0.56488 at 0.043112 standard deviations. The mesh growth rate i.e element size of the blade subdomain to the blade edge was increased by 1.2 and its geometry consists of 401,877 nodes and 796,507 elements when the blade edges element sizes were 0.001 as several divisions.

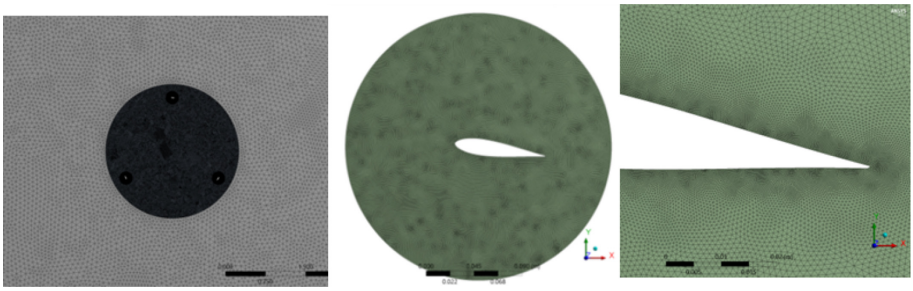

Fig. 5. Mesh generations; full domain, zoomed blade sub-domain, and around blade edges (left to right).

Solution Setup. A 2D pressure-based U-RANS formulation is used for numerical simulation and is a suitable solver for time-dependent analysis [28]. To capture implicit velocity-pressure coupling SIMPLE algorithms with the second-order upwind scheme were selected for the spatial discretization method using finite volume analysis [29, 30], which was executed for the unsteady simulations with good resolution. To compute dynamic force and unsteady flow field sliding mesh approach was used to behold the flow physics of the rotating and blade subdomain [6, 29]. This effectively computes the relative motion between fixed and rotating domains by interpolating the domain's flow quantity under transient conditions.

3.3 Models Validation

Once an optimized simulation is done, immediate comparisons were performed with experimental scientific pieces of literature which were conducted on small scale VAWT. The turbine design specifications are presented in Table 3 the torque calculated by CFD simulations well agreed with Yang et al. [36] presented in Fig. 6. Except for a little overestimation of the current investigations the results are well agreed with the previous work. This delay was due to the 3D simulation effect at low TSR rather than the airfoil type used (Table 2).

Table 2. Comparison literatures.

Dimensions	N	c (m)	l(m)	S(m^2)	V (m/s)	Airfoil type
I. Paraschivoiu; 2002 [25] (Sandia 2m)	3	2	5.877	2.5944	variable	NACA0012
Yang et al.; 2018 [36]	2	2	0.265	2.4	8	NACA0021

Similarly, Fig. 6 and 7 demonstrates both results in the present study (i.e. DMST and CFD at $\lambda = 2.5$) are agreed each other except some bet of delay was observed on the CFD side. In general, it is logical to say the present numerical results well agreed with Sandia 2 m wind tunnel result [25], considering multiple loss factors and the present design parametric advantages i.e. airfoil type, VP-blade design, and 2D effect.

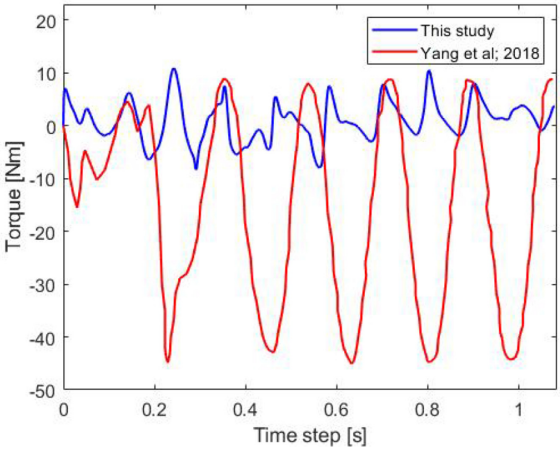

Fig. 6. A turbine torques comparisons.

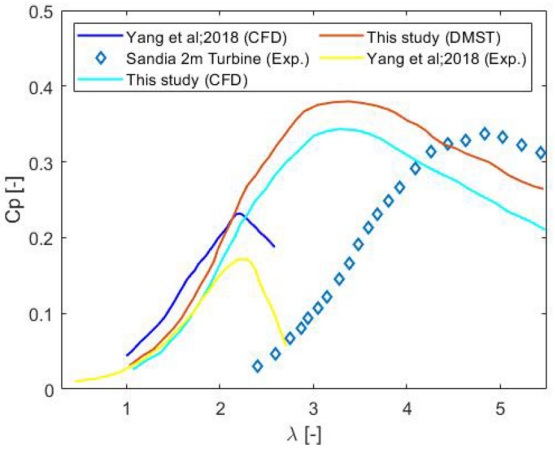

Fig. 7. Power coefficients comparisons.

4 Results and Discussions

4.1 Effect of Airfoil and Reynolds Number

Reynolds number (Re) plays a significant role in the performance of VAWT. The lower Re suffers turbine performance slope degradations and which leads the turbine unable to self-start. Hence, the turbine Reynolds number effect on the lift generation was done for five different airfoils presented in Fig. 8. At the same instant of chord (c) length, the performance comparison of airfoils was done within Reynolds number range 2.5×10^5

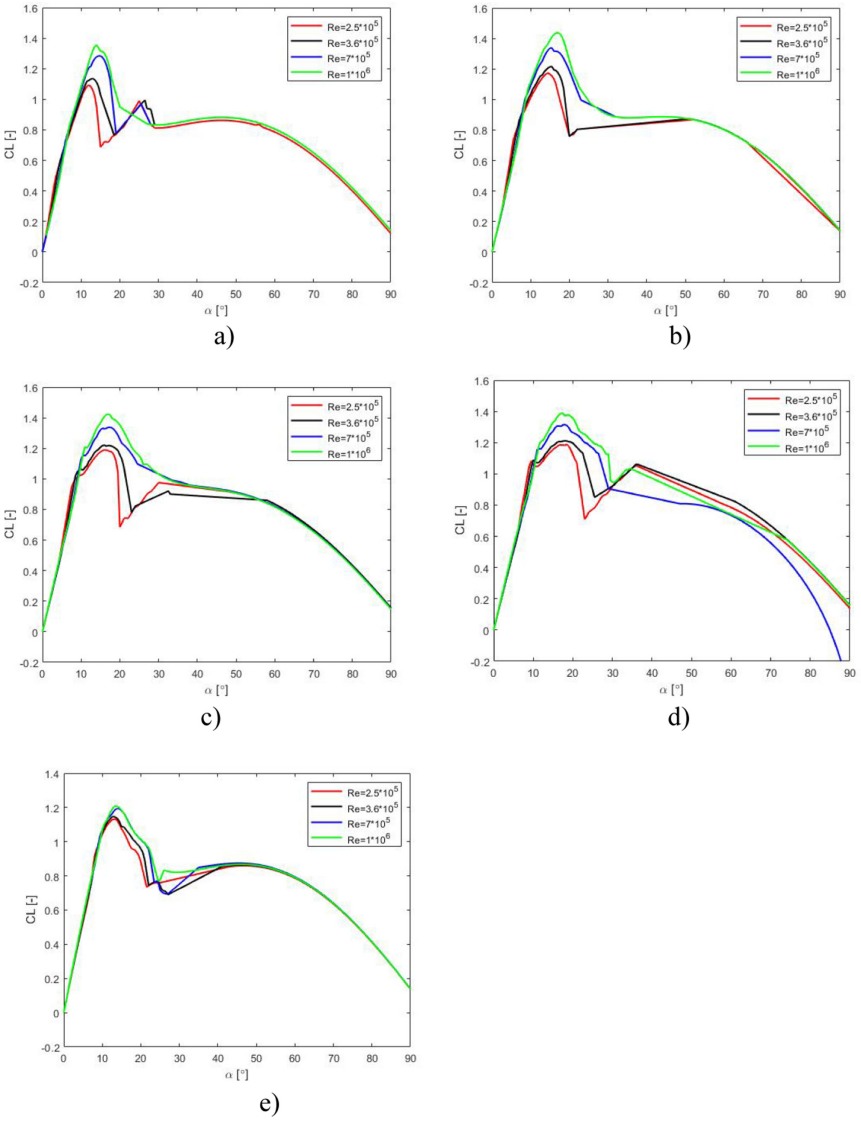

Fig. 8. Reynolds numbers affect different airfoils. a) NACA0012 b) NACA0015 c) NACA0018 d) NACA0021 e) S1046

to 1×10^6. The result shows that CL was increasing with Reynolds number until stall angle of attack. It demonstrated; all NACA-series airfoils are highly sensitive to Re values, and these are agreed with the result presented in [4]. While the lift coefficient of the S1046 airfoil is no longer disturbed with the change in operating Reynolds number because S1046 airfoil profile crossover NACA-series airfoils at the same camber scale.

According to Fig. 8 NACA0015 is the best performance at a high Reynolds number ($Re \geq 7 \times 10^5$) since it has a higher lift coefficient (CL). However, the detached flow has occurred at a low angle of attack (α) and it can be confirmed that S1046 airfoils offer a higher lift coefficient (CL) at a low Reynolds number ($2.5 \times 10^5 \leq Re\ 3.6 \times 10^5$). This shows S1046 airfoil significantly suppressed the flow separation at low AoA and augments the turbine performance.

4.2 Turbine Loading Conditions

Figure 9 comprises the simulation tangential force coefficient of the examined rotor with the design parameters presented in Table 1, from $-90°$ to $270°$ azimuth angles at an approximate TSR between 1.285 and 5.4. disregarding the dynamic stall effect, the results are agreed with the previously studied VAWT loading conditions [25, 37]. The maximum tangential force coefficients in the upwind and downwind sides of the present study were obtained at $-10°$ and $170°$ azimuth angles respectively. The instantaneous tangential force coefficients corresponding to upwind and downwind sides in the previous studies occurred at $10°$ and $210°$ azimuth angles respectively [25, 37]. However, deviations have occurred on both sides of the rotor. This is since the airfoil profile used in the study affects blade instantaneous loadings. Generally, the simulation gives suitable results at different combinations of TSR and pitch angles.

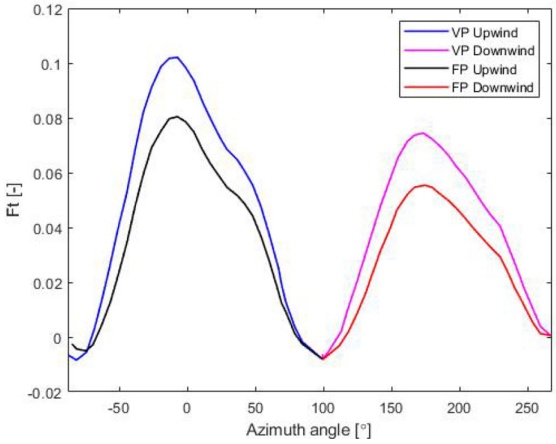

Fig. 9. Tangential Force coefficient at different azimuth positions.

4.3 The Turbine Self-starting

Figure 10 demonstrates the performance of the turbine with emphasis was computed by the proposed implementations under the range of −5° to 5° pitch angle (β). The minimum simulated self-starting power coefficient (0.1691) was obtained at low TSR (λ = 2.0769) when the blades are fixed at a 3° pitch angle. This is approximated to the conventional performance of small-scale vertical axis wind turbines (i.e. C_P = 0.17). The maximum performance (C_P = 0.45) was determined at λ = 3 and 3° of β. But a small increment in β (approximately3°) reveals a significant increment in the C_P up to the limit of VAWT performance, I.Paraschivoiu (64% V∞) [25]. Hence, C_P is significantly dependent on the blade pitch angle (β). Similar effects of blade pitch angles on VAWT performance are presented in [37] which are in agreement with the current findings.

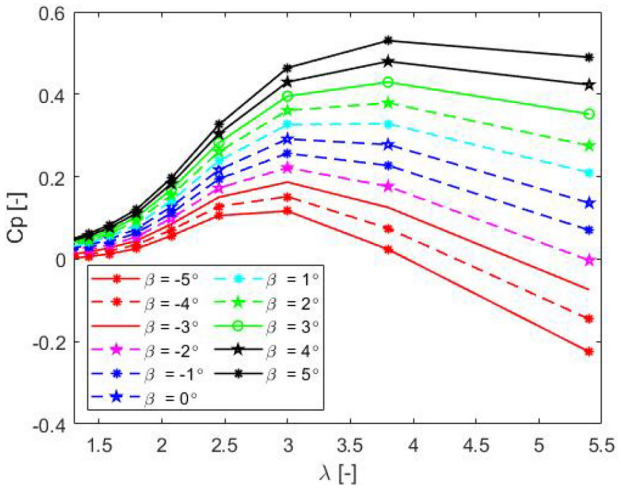

Fig. 10. Power coefficients at different pitch angles.

4.4 The Moment Coefficient (Cm) of the Turbine

Table 3 shows the optimum parametric presiding design point's obtained from the DMST model for CFD simulations. The process starts setting the rotational velocity of the turbine (ω) and then calculating the time step required to rotate one degree, Eq. (25), taking into account the relation between radians and degrees. This implies that for the whole range of TSR values from which we want to obtain the turbine performance, the time step must be changed accordingly. Figure 11 demonstrates the performance comparisons of VAWT with fixed and variable blade pitch angles which are obtained from CFD simulations. As was expected, the highest turbine performance was obtained when the blade is configured at a positive pitch angle. In the case of fixed pitch (β = 0°), the minimum and maximum C_m at DP3 were −0.071 and 0.0703 respectively. Under a similar simulation parameter (i.e. DP3), when the blade pitch

angle varied to 3° (see Fig. 11c), the minimum and maximum rotor performance rose to −0.0409 and 0.15714 respectively.

$$\Delta t_{1^o} = \frac{1}{\omega(rps) \times 360} \tag{25}$$

Table 3. Rotor speed with a corresponding time steps.

Design point (DPs)	Rotor speed (rad/s)	Time step sizes (s)	TSR [-]
DP1	7.2	0.000385802469	1
DP2	14.4	0.000771604938	2
DP3	21.6	0.001157407407	3

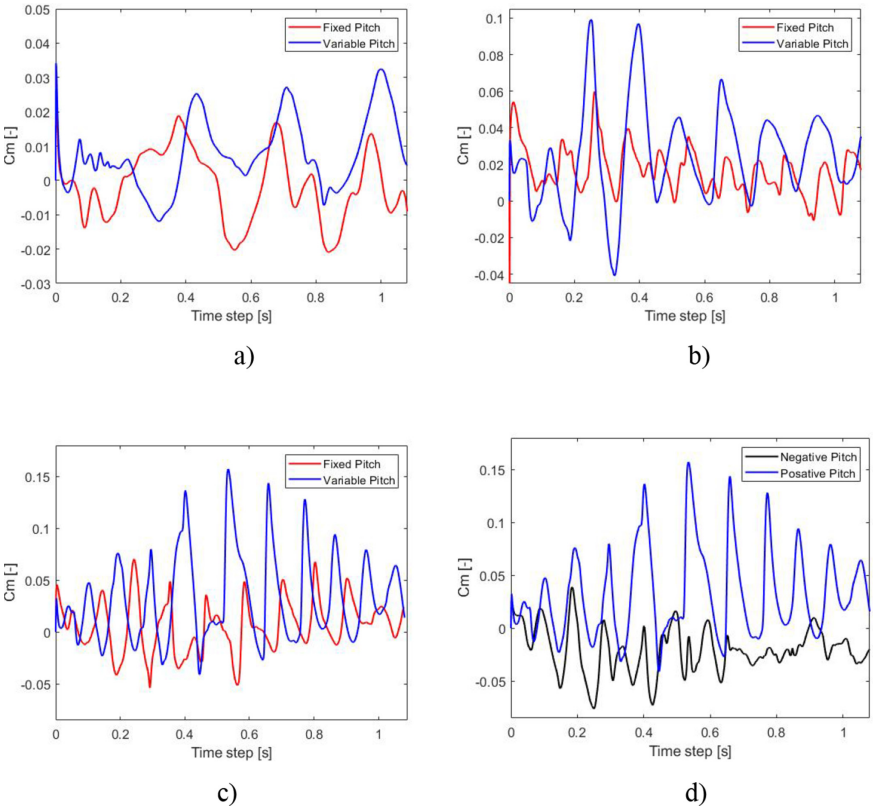

Fig. 11. Moment coefficients at different TSR. a) λ = 1 b) λ = 2 c) λ = 3 d) positive pitch (λ = 3) and negative pitch (λ = −3)

This shows that the turbine blade with a 3° pitch angle offered the maximum moment coefficient (Cm = 0.16) which is 37.2% higher than the turbine at zero pitch angle (Cm = 0.07). This shows blade pitching at a larger positive angle decelerates the turbine flow separation which occurred at low AoA and it enables the turbine to self-start. Next, the use of negative pitch angle (β = −3°) of the turbine blade was investigated. As can be seen in Fig. 11d, the rotor performance with inward (negative) and outward (positive) pitch angles are computed. It can be shown that blades with a positive pitch angle of 3° afforded a better performance improvement at every time step. This shows that the H-Darrieus rotor with positive blade pitch angle plays a significant role in the performance alleviation than negative pitch once. In addition to that, the rotor performance was depending upon its TSR. It indicates the turbine performance was slightly increased with TSR. Even though the performance was lower at TSR (λ = 1) (Fig. 11a), VP-rotor provides early starting at the initial time step.

4.5 Pressure Distributions of the Turbine Blades

Unsteady pressure and velocity contours have been plotted to understand the flow physics of the H-Darrieus wind turbine at two different pitch angles (i.e. 0° and 3°). Also, Fig. 12 and 13 demonstrate the velocity and pressure contours of the H-Darrieus rotors in the two different blade configurations. In the case of the FP rotor, the global pressure contour was at the range of (2.264 × 10)^2 to –(9.168 × 10)^2 Pa (Pa).

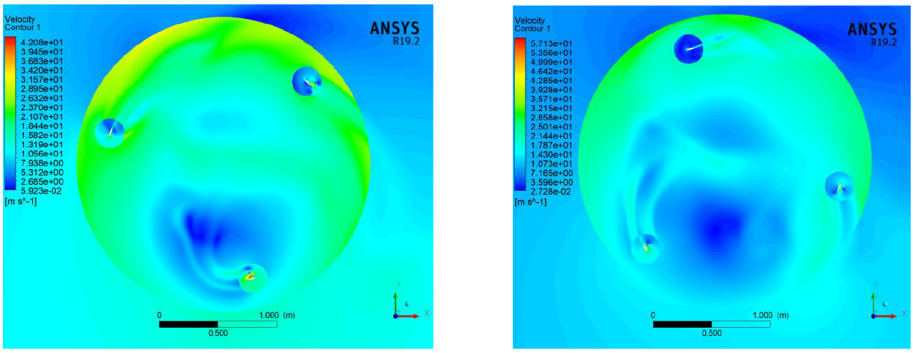

a) b)

Fig. 12. Velocity contours. a) Fixed pitch b) Variable pitch

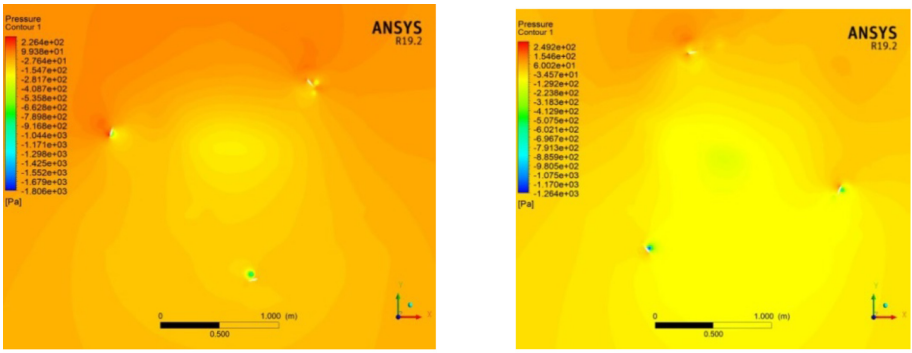

a) b)

Fig. 13. Pressure contour. a) Fixed pitch b) Variable pitch

5 Conclusion

The current study reveals the performance analysis of straight blade H-Darrieus VAWT using DMST and CFD models. The important aspects of these studies include airfoil profile, optimum rotor design points, and blade pitch angles with TSR. Additionally, 2D unsteady flow with the same airfoil was also analyzed using CFD. All these results are analyzed to make a clear performance comparison between FP and VP H-Darrieus VAWT and the result was validated with numerical and wind tunnel experimental studies. The following conclusions are drawn:

- S1046 airfoil provides a higher lift-drag ratio than the other symmetrical NACA-sires airfoils used in this study. This is because the thickness of the S1046 airfoil reduces flow separation and its performance is no longer disturbed with the change in operating Reynolds number.
- Instantaneous aerodynamic loads (tangential force coefficient) acting on the upwind side of the rotor is higher than the downwind side once. This is because of the free-stream wind velocity reduced by upstream and downstream induction factors consecutively.
- The minimum performance (CP = 0.1691) requirements to enabling the rotor for self-starting at low TSR was obtained at the outward blade pitch angle ($\beta = 3°$). While at the same aerodynamic conditions but with blades in inward pitch angle ($\beta = -3°$) the corresponding rotor performance becomes too low. Hence, positive pitch angles exhibited superior performance than negative blade pitch angles.
- From the flow physics of the rotor, it has been seen that the greater pressure difference across VP-blades meaning enhanced aerodynamic performance of this rotor.

The present study has shown that small-scale symmetrical S1046 airfoil straight blade H-Darrieus rotor with VP configuration possess higher power coefficient and moment coefficients than FP blade. Once the present design will be scaled up or modified with a 3D-CFD model then future researchers can compare their findings with this work.

References

1. Johari, M., Jalil, M., Mohd Shariff, M.: Comparison of horizontal axis wind turbine (HAWT) and vertical axis wind turbine (VAWT). Int. J. Eng. Technol. **7**(4.13), 74–80 (2018)
2. Saad, M.M.M., Asmuin, N.: Comparison of horizontal axis wind turbines and vertical axis wind turbines. IOSR J. Eng. (IOSRJEN) **4**(08), 27–30 (2014)
3. Hameed, M.S., Afaq, S.K.: Design and analysis of a straight bladed vertical axis wind turbine blade using analytical and numerical techniques. Ocean Eng. **57**, 248–255 (2013)
4. Bogateanu, R., Dumitrache, A., Dumitrescu, H., Stoica, C.I.: Reynolds number effects on the aerodynamic performance of small VAWTs. Sci. Bull. Univ. "Politeh" Bucharest, Ser. D **76** (1), pp. 25–36 (2014)
5. Armstrong, S., Fiedler, A., Tullis, S.: Flow separation on a high Reynolds number, high solidity vertical axis wind turbine with straight and canted blades and canted blades with fences. Renew. Energy **41**, 13–22 (2012)
6. Hashem, I., Mohamed, M.: Aerodynamic performance enhancements of H-rotor Darrieus wind turbine. Energy **142**, 531–545 (2018)
7. Islam, M., Fartaj, A., Carriveau, R.: Analysis of the design parameters related to a fixed-pitch straight-bladed vertical axis wind turbine. Wind Eng. **32**(5), 491–507 (2008)
8. Kirke, B., Lazauskas, L.: Limitations of fixed pitch Darrieus hydrokinetic turbines and the challenge of variable pitch. Renew. Energy **36**(3), 893–897 (2011)
9. Kirke, B., Lazauskas, L.: Enhancing the performance of vertical axis wind turbine using a simple variable pitch system. Wind Eng. **15**(4), 187–195 (1991)
10. Paraschivoiu, I., Trifu, O., Saeed, F.: H-Darrieus wind turbine with blade pitch control. Int. J. Rotating Mach. **2009** (2009). https://doi.org/10.1155/2009/505343
11. Shuqin, L.: Magnetic suspension and self-pitch for vertical-axis wind turbines. Fundam. Adv. Top. Wind Power, 233–248 (2011). https://doi.org/10.5772/22598
12. Hwang, I.S., Min, S.Y., Jeong, I.O., Lee, Y.H., Kim, S.J.: Efficiency improvement of a new vertical axis wind turbine by individual active control of blade motion. In: Smart Structures and Materials 2006: Smart Structures and Integrated Systems, vol. 6173, p. 617311. International Society for Optics and Photonics (2006)
13. Paraschivoiu, I.: Double-multiple streamtube model for studying vertical-axis wind turbines. J. Propul. Power **4**(4), 370–377 (1988)
14. Ayati, A.A., Steiros, K., Miller, M.A., Duvvuri, S., Hultmark, M.: A double-multiple streamtube model for vertical axis wind turbines of arbitrary rotor loading. Wind Energy Sci. **4**(4), 653–662 (2019)
15. Manwell, J.F., McGowan, J.G., Rogers, A.L.: Wind Energy Explained: Theory, Design and Application. Wiley (2010)
16. Zhao, Z., et al.: Study on variable pitch strategy in H-type wind turbine considering effect of small angle of attack. J. Renew. Sustain. Energy **9**(5), 053302 (2017)
17. Zhao, Z., et al.: Variable pitch approach for performance improving of straight-bladed VAWT at rated tip speed ratio. Appl. Sci. **8**(6), 957 (2018)
18. Mohamed, M., Ali, A., Hafiz, A.: CFD analysis for H-rotor Darrieus turbine as a low speed wind energy converter. Eng. Sci. Technol. Int. J. **18**(1), 1–13 (2015)
19. Ghasemian, M., Ashrafi, Z.N., Sedaghat, A.: A review on computational fluid dynamic simulation techniques for Darrieus vertical axis wind turbines. Energy Convers. Manage. **149**, 87–100 (2017)
20. Li, Q.A., Maeda, T., Kamada, Y., Hiromori, Y., Nakai, A., Kasuya, T.: Study on stall behavior of a straight-bladed vertical axis wind turbine with numerical and experimental investigations. J. Wind Eng. Ind. Aerodyn. **164**, 1–12 (2017)

21. Castelli, M.R., De Betta, S., Benini, E.: Effect of blade number on a straight-bladed vertical-axis Darreius wind turbine. World Acad. Sci. Eng. Technol. **61**, 305–311 (2012)
22. Beri, H., Yao, Y.: Double multiple streamtube model and numerical analysis of vertical axis wind turbine. Energy Power Eng. **3**(03), 262 (2011)
23. Saber, E., Afify, R., Elgamal, H.: Performance of SB-VAWT using a modified double multiple streamtube model. Alex. Eng. J. **57**(4), 3099–3110 (2018)
24. Paraschivoiu, I.: Double-multiple streamtube model for Darrieus in turbines (1981)
25. Paraschivoiu, I.: Wind Turbine Design: with Emphasis on Darrieus Concept. Presses Inter Polytechnique (2002)
26. Mohammed, A.A., Ouakad, H.M., Sahin, A.Z., Bahaidarah, H.: Vertical axis wind turbine aerodynamics: summary and review of momentum models. J. Energy Resour. Technol. **141** (5), 050801 (2019)
27. Du, L., Ingram, G., Dominy, R.G.: Experimental study of the effects of turbine solidity, blade profile, pitch angle, surface roughness, and aspect ratio on the H-Darrieus wind turbine self-starting and overall performance. Energy Sci. Eng. **7**(6), 2421–2436 (2019)
28. Balduzzi, F., Bianchini, A., Maleci, R., Ferrara, G., Ferrari, L.: Critical issues in the CFD simulation of Darrieus wind turbines. Renew. Energy **85**, 419–435 (2016)
29. Alqurashi, F., Mohamed, M.: Aerodynamic forces affecting the H-Rotor Darrieus wind turbine. Modell. Simul. Eng. **2020** (2020)
30. Nguyen, M.T., Balduzzi, F., Bianchini, A., Ferrara, G., Goude, A.: Evaluation of the unsteady aerodynamic forces acting on a vertical-axis turbine by means of numerical simulations and open site experiments. J. Wind Eng. Ind. Aerodyn. **198**, 104093 (2020)
31. Wang, Y., Shen, S., Li, G., Huang, D., Zheng, Z.: Investigation on aerodynamic performance of vertical axis wind turbine with different series airfoil shapes. Renew. Energy **126**, 801–818 (2018)
32. Mazarbhuiya, H.M.S.M., Biswas, A., Sharma, K.K.: Low wind speed aerodynamics of asymmetric blade H-Darrieus wind turbine-its desired blade pitch for performance improvement in the built environment. J. Braz. Soc. Mech. Sci. Eng. **42**(6), 1–16 (2020). https://doi.org/10.1007/s40430-020-02408-0
33. Menter, F.R., Langtry, R.B., Likki, S., Suzen, Y., Huang, P., Völker, S.: A correlation-based transition model using local variables—part I: model formulation (2006)
34. Castelli, M.R., Dal Monte, A., Quaresimin, M., Benini, E.: Numerical evaluation of aerodynamic and inertial contributions to Darrieus wind turbine blade deformation. Renew. Energy **51**, 101–112 (2013)
35. Kavade, R.K., Ghanegaonkar, P.M.: Performance evaluation of small-scale vertical axis wind turbine by optimized best position blade pitching at different tip speed ratios. J. Inst. Eng. (India) Ser. C **100**(6), 1005–1014 (2019)
36. Yang, Y., Guo, Z., Song, Q., Zhang, Y., Li, Q.A.: Effect of blade pitch angle on the aerodynamic characteristics of a straight-bladed vertical axis wind turbine based on experiments and simulations. Energies **11**(6), 1514 (2018)
37. Vitale, A.J., Genchi, S.A., Rossi, A.P., Guillermo, E.D., di Prátula, H.R.: Aerodynamic performance of straight-bladed vertical axis wind turbines: a practical open source implementation. Int. J. Renew. Energy Res. (IJRER) **8**(2), 1025–1037 (2018)